9.9 A High-Efficiency 28GHz Outphasing PA with 23dBm Output Power Using a Triaxial Balun Combiner

Bagher Rabet[1], James Buckwalter[2]

[1]University of California, San Diego, La Jolla, CA
[2]University of California, Santa Barbara, Santa Barbara, CA

Gigabit-per-second millimeter-wave (mm-wave) access and backhaul networks at 28GHz demand high-order QAM, OFDM, and/or carrier-aggregated waveforms that force the PA to operate under high peak-to-average power ratio (PAPR) [1]. High PAPR requirements aggravate the design of mm-wave Si CMOS and SiGe BiCMOS PAs since a linear response and high efficiency are simultaneously desired. Recent work has demonstrated mm-wave PAs with peak efficiency exceeding 30% at 28GHz for output powers above 20dBm [1-5]. However, high average efficiency associated with high-PAPR waveforms remains elusive. To improve average efficiency, circuit techniques based on Doherty [3] and outphasing [6] have been demonstrated in mm-wave bands. Earlier work using these techniques showed average efficiency with QAM waveforms that is well under 20%.

In this paper, we present a SiGe BiCMOS outphasing power amplifier (OPA) with substantially better performance due to an extremely low-loss power combiner that realizes both excellent peak power-added-efficiency (PAE) of 41% and average PAE of 25.3% for an 8.1dB-PAPR signal at 28GHz. The power combiner is based on a compact triaxial balun structure that simultaneously generates the Chireix compensating reactances at the output ports of the PAs for load modulation and combines the RF power with low loss.

The conventional Chireix OPA is shown in Fig. 9.9.1. The PAs drive the combiner with constant-envelope signals separated by an outphasing angle ($\pm\varphi$). The load seen by each PA is modulated through a non-isolating power combiner, shown here as a transformer, along with the opposite-signed Chireix reactances ($\pm jX_{CH}$) at each of the combiner ports. Previous work investigated the Chireix OPA in mm-wave bands with limited success to realize high average efficiency [6]. Two significant challenges exist for CMOS/BiCMOS PAs in mm-wave bands. First, high losses in the on-chip power combiners significantly reduce the gain, output power, and any theoretical average efficiency improvement. Second, the typical OPA requires a voltage-mode PA that is difficult to realize at mm-wave frequencies due to the relative admittance presented by device parasitics.

The proposed OPA is also shown in Fig. 9.9.1 and replaces the conventional Chireix combiner with a triaxial balun that combines the outputs of the two PAs while inherently producing the compensating reactances and providing impedance match to the load with low loss. The PA cell is also illustrated in Fig. 9.9.1 based on a 0.13µm SiGe HBT cascode where the output capacitance is roughly 85fF. The cascode base is biased with low impedance to sweep out the carriers generated from impact ionization, thereby improving the breakdown for increased output power. The transistor emitter lengths are sized to create a loadline impedance that optimizes the efficiency and output power over the range of impedances seen by the triaxial balun. The PA cell produces 20.5dBm and a maximum PAE of 47% based on post-layout simulation. While the PA cells present a large output impedance to the combiner compared to the canonical voltage source in a general outphasing approach, the amplitude and phase difference of the input signals (S_1 and S_2) are modified to maintain high efficiency over a range of output powers.

The triaxial balun is conceptually illustrated in Fig. 9.9.2 and indicates two inner conductors connected to the input ports (P_1 and P_2) and an outer conductor that serves as a return path (ground) for the current from the output port that is connected to a load impedance R_L [7]. The characteristic impedance Z_{0_IN} between P_1 and P_2 is designed independently of the characteristic impedance Z_{0_OUT} between P_2 and ground. As shown in the equivalent RF circuit, the Z_{0_IN} provides output matching of the triaxial balun while Z_{0_OUT} produces a shunt reactance on P_2. Therefore, the impedances produced by the triaxial balun can be related to the design of the Chireix outphasing scheme as shown in Fig. 9.9.2. The PA cell's output capacitance is absorbed into the Chireix network while the length of the balun is chosen to produce the desired shunt inductance on one of the PA outputs. Thus, a relatively short length, e.g. $l = \lambda/16$, transmission line is required for the outphasing combiner, resulting in low loss.

The balun equivalent model captures the RF behavior precisely, but slight adjustments are needed to capture the DC behavior. Each PA cell has a DC voltage supply provided through the triaxial balun. The cell connected to P_2 is fed directly from the alternate end of the conductor with AC short provided by local bypass capacitors (not shown in figure). The cell connected to P_1 can be fed via a DC-feed inductor at any point along the inner conductor. In this work, a wirebond connecting one of the DC pads to the output RF pad provides this inductor.

In Fig. 9.9.3, the triaxial balun, as implemented in a planar integrated circuit process, is shown. P_1 is the central conductor while P_2 is the shield around P_1 to form a microstrip structure, and the return path is through the ground conductor on either side of P_2. A fabricated back-to-back test structure indicates that the measured insertion loss of the combiner is 0.52dB and is close to the simulated value of 0.35dB around 28GHz. Furthermore, Fig. 9.9.3 shows the impedances seen at P_1 and P_2 as a function of outphasing angle, which matches the canonical outphasing load modulation. The loads corresponding to the PA cell's peak output power and efficiency, denoted R_{L_Pout} and R_{L_PAE}, are traversed by the outphasing impedance trajectories.

The simulated and measured gain, collector efficiency (η), and PAE are plotted in Fig. 9.9.4. The input signals for testing are equi-amplitude with opposite phase. An initial sweep is performed to determine the optimal amplitude and phase for maximum efficiency. The measured small-signal gain is 14dB. The peak output power is 23dBm with corresponding PAE of 35.5%. The peak PAE of 41% is reached at 21dBm while the collector efficiency reaches 44%. The PAE measured at 6dB backoff relative to the maximum power of 23dBm is 34.7%. Additionally, corroboration between simulation and measurement is excellent over the entire range of output power.

The OPA was tested with an 80MHz 64-QAM OFDM signal with PAPR of 8.1dB at 28 GHz as shown in Fig. 9.9.5. Equalization is applied to the entire test setup including the PA. The average output power with modulation is 14.3dBm and the RMS EVM of 3% is achieved with the use of a memoryless DPD algorithm. The average PAE for the OFDM signal is 25.3%. The adjacent-channel power leakage, also shown in Fig. 9.9.5, indicates that the relative power 60MHz away from the band edge is less than -33dBc.

Figure 9.9.6 compares the proposed OPA with state-of-the-art PA performance at 28GHz. This work achieves high output power, peak efficiency, and most notably, the highest 6dB-power-backoff PAE at 34.7% compared to prior work. Furthermore, the modulation measurement demonstrates that the PA can achieve excellent EVM at a high average output power with the assistance of memoryless DPD. Additionally, the average PAE for the QAM waveform is the highest average efficiency for a mm-wave PA and demonstrates the potential for fully integrated PAs that can efficiently support high-PAPR waveforms at 28GHz. The die micrograph is shown in Fig. 9.9.7. The PA area, including pads and input routing, is 700um×800um and the chip operates from a 4V supply.

Acknowledgements:
The authors thank P. Maki of ONR for support of this work and N. Cahoon of GlobalFoundries for chip fabrication. Additionally, the authors thank Prof. D. Sievenpiper, Prof. P. Asbeck, H. Gheidi, and C. Levy of UCSD. We appreciate the donation of EMX software from Integrand.

References:
[1] S. Shakib, et al., "A Wideband 28GHz Power Amplifier Supporting 8×100MHz Carrier Aggregation for 5G in 40nm CMOS," *ISSCC*, pp. 44-45, Feb. 2017.
[2] A. Sarkar, et al., "A 28-GHz SiGe BiCMOS PA with 32% Efficiency and 23-dBm Output Power," *IEEE JSSC*, vol. 52, no. 6, pp. 1680-1686, June 2017.
[3] S. Hu, et al., "A 28GHz/37GHz/39GHz Multiband Linear Doherty Power Amplifier for 5G Massive MIMO Applications," *ISSCC*, pp. 32-33, Feb. 2017.
[4] S. Shakib, et al., "A 28GHz Efficient Linear Power Amplifier for 5G Phased Arrays in 28nm Bulk CMOS," *ISSCC*, pp. 352-353, Feb. 2016.
[5] A. Sarkar and B. A. Floyd, "A 28-GHz Harmonic-Tuned Power Amplifier in 130-nm SiGe BiCMOS," *IEEE TMTT*, vol. 65, no. 2, pp. 522-535, January 2017.
[6] D. Zhao, et al., "A 60GHz Outphasing Transmitter in 40nm CMOS with 15.6dBm Output Power," *ISSCC*, pp. 170-171, Feb. 2012.
[7] H.-C. Park, et al., "Millimeter-Wave Series Power Combining Using Sub-Quarter-Wavelength Baluns," *IEEE JSSC*, vol. 49, pp. 2089-2102, 2014.

 978-1-5090-4940-0/18/$31.00

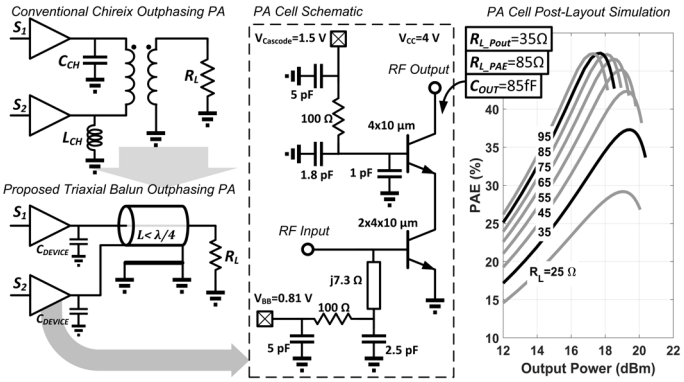

Figure 9.9.1: Block diagram comparing a conventional Chireix outphasing PA and proposed triaxial balun outphasing PA. Illustration of proposed HBT PA cell and PAE simulations.

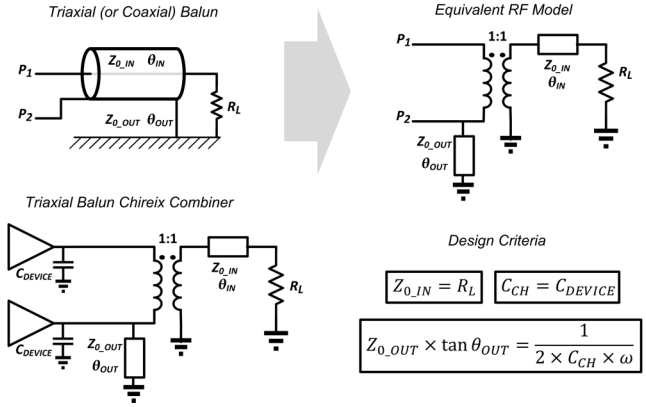

Figure 9.9.2: Conceptual representation of the triaxial balun and equivalent RF circuit as related through design criteria to the outphasing PA.

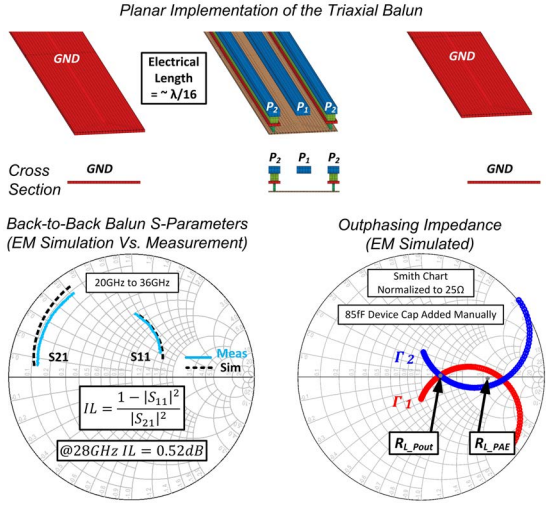

Figure 9.9.3: Implementation of the planar triaxial balun and comparison of simulation and measurement for a back-to-back balun. Simulation of the resulting load modulation on the PA cells.

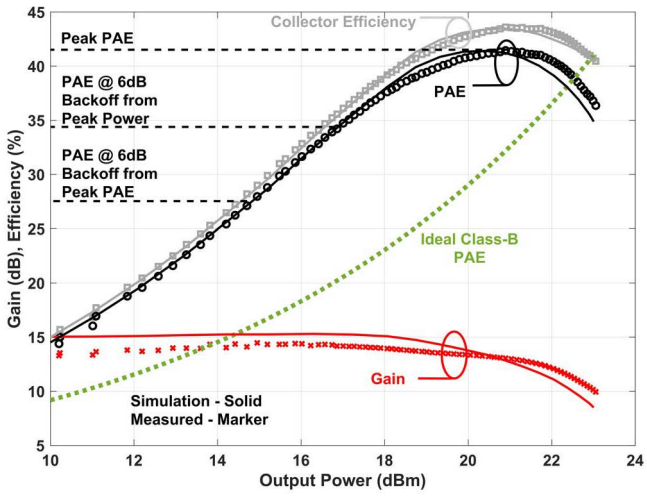

Figure 9.9.4: Comparison of simulated and measured efficiency and gain alongside an ideal Class-B response. The efficiency improvement at backoff is evident.

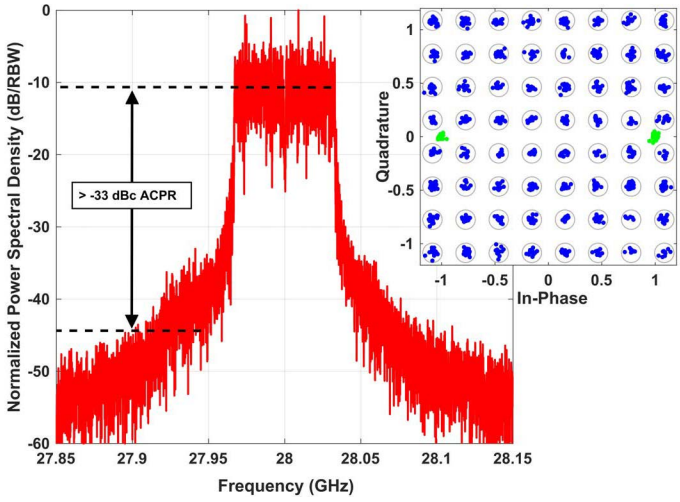

Figure 9.9.5: Illustration of the spectrum, ACPR, and constellation for an 80MHz 64-QAM OFDM signal with average output power of 14.3dBm. The measured EVM is -30.5dB and average PAE is 25.3%.

TABLE I

COMPARISON WITH THE STATE OF THE ART

	[4]	[1]	[3]	This work
Frequency (GHz)	30	27	28	28
Technology	28nm CMOS	40nm CMOS	130nm SiGe	130nm SiGe
P_{SAT}(dBm)	15.3	15.1	16.8	**23**
Peak PAE (%)	36.6	33.7	20.3	**41.4**
PAE @ 6dB from P_{SAT}	NA	15.1	13.9	**34.7**
Modulation Type	64 QAM OFDM	64 QAM OFDM	64QAM Single Carrier	64 QAM OFDM
PAPR (dB)	9.6	9.7 (clipped to 8.4)	NA	8.1
Signal BW (MHz)	250	800	500 / 1000	80
Pre-distortion	No	No	No	Memoryless DPD
Average Pout (dBm)	5.3	6.7	9.2 / 7.2	**14 .3**
EVM (dB)	-25	-25	-27 / -26.6	-30.5
Average PAE (%)	9.6	11	18.5* / 14.4*	**25.3**

* Collector Efficiency (not PAE)

Figure 9.9.6: Table of comparison with recent 28GHz PAs.

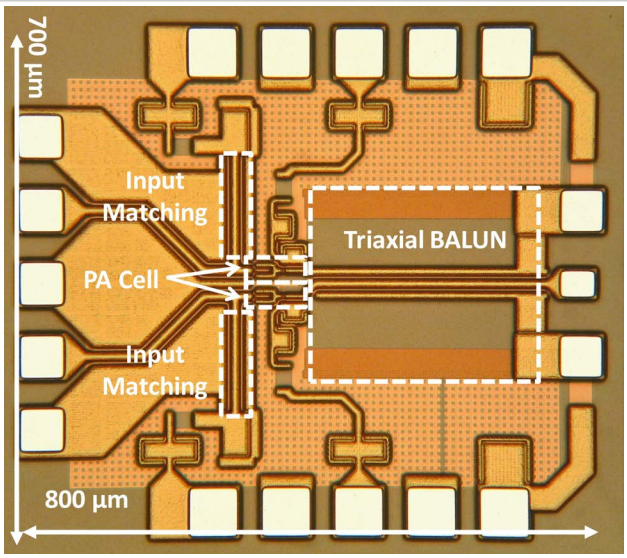

Figure 9.9.7: Die micrograph of the PA circuit.

978-1-5090-4940-0/18/$31.00